CFD Letters

Journal homepage:
https://semarakilmu.com.my/journals/index.php/CFD_Letters/index
ISSN: 2180-1363


# The Soret-Dufour Effects on Three-Dimensional Magnetohydrodynamics Newtonian Fluid Flow over an Inclined Plane

Siti Suzilliana Putri Mohamed Isa[1,2*], Hazirah Mohd Azmi[1], Nanthini Balakrishnan[1], Aina Suhaiza Mohamad Nazir[2], Kartini Ahmad[3], Nurul Syuhada Ismail[4], Norihan Md. Arifin[5], Haliza Rosali[5]

[1] Institute for Mathematical Research, Universiti Putra Malaysia, 43400 UPM Serdang, Selangor Darul Ehsan, Malaysia
[2] Centre of Foundation Studies for Agricultural Science, Universiti Putra Malaysia.43400 UPM Serdang, Selangor Darul Ehsan, Malaysia
[3] Department of Science in Engineering, Kulliyah of Engineering, International Islamic University Malaysia, 50728 Gombak, Kuala Lumpur, Malaysia
[4] Centre for Pre – University Studies, Universiti Malaysia Sarawak, 94300, Kota Samarahan, Sarawak, Malaysia
[5] Department of Mathematics, Faculty of Science, Universiti Putra Malaysia, 43400 UPM Serdang, Selangor Darul Ehsan, Malaysia

**ARTICLE INFO**

***Article history:***
Received 4 November 2023
Received in revised form 8 December 2023
Accepted 7 January 2024
Available online 30 April 2024

***Keywords:***
Soret-Dufour; magnetohydrodynamics; Newtonian fluid; 3D model; Matlab bvp4c

**ABSTRACT**

The three-dimensional (3D) model of the fluid flow model with length, breadth, and height or depth is the advanced and precise version from the two-dimensional (2D) model which just lies on a flat surface. The heat transfer in the boundary layer flow have numerous applications in the production of polymer, plastic films, and paper production. Therefore, this paper solves 3D magnetohydrodynamics Newtonian fluid flow model with the effect of Soret-Dufour parameters. Compared with the previous report where the 3D model is without the inclination angle (all the axes are located at their fixed position), this paper considers the boundary xy-plane being projected by a certain angle from the z-axis. The initial partial differential equations (PDEs) are subsequently reduced to ordinary differential equations (ODEs). The MATLAB bvp4c program is chosen to solve the ODEs and the results velocity profile, temperature profile, concentration profile, skin friction coefficient, local Nusselt number, and local Sherwood number. It can be inferred that the magnetic parameter is responsible to the decrement of the velocity profile and skin frictions coefficient. The enhancement of the temperature and the local Sherwood number are caused by the Dufour number. Besides, concentration and the local Nusselt number are enhancing due to the increasing Soret number.

## 1. Introduction

Research in magnetohydrodynamic (MHD) boundary flow has captured significant deliberation due to its relevant applications such as in MHD generators, refrigeration, or warming applications, etc. As compared to the two-dimensional flow as reported recently, the three-dimensional (3D) dimension is more realistic and practical in application. As such, several authors take the effort to investigate 3D MHD flow such as stretching/shrinking plate [1-4] and rotating stretching/shrinking

* *Siti Suzilliana Putri Mohamed Isa*
*E-mail address: ctsuzilliana@upm.edu.my (Siti Suzilliana Putri Mohamed Isa)*

https://doi.org/10.37934/cfdl.16.9.3951

sheet [5-7]. However, these studies [1-7] are limited to flows moved over a horizontal/vertical stretching sheet. They develop a plate without any inclination from any axis. The fluid flows over an inclined sheet were reported for the MHD model [8-12] are with these controlling factors: when the fluid state is unsteady [8], with the Newtonian heating effect [9], the fluid model considers the free convection flow [10], the fluid is bounded by the slip condition [11], with the presence of porous medium [11, 13], or when the stagnation point is existed in the fluid flow [12]. The boundary layer flow bounded by an inclined sheet observes the characteristics of the fluid flow when the sheet can be displaced by a certain angle by the same origin point, instead of the static sheet.

It is worth mentioning that most of the works cited above are with the absence of Soret and Dufour effects. Temperature gradient causes the occurrence of diffusion flux known as Soret effect (thermal diffusion), whilst chemical potential gradient results in the occurrence of heat flux noted as Dufour effect. Such impacts are very much significant in hydrology, petrology, nuclear reactors, etc [14]. The Soret-Dufour effects in the fluid flow model is developed when the vector of magnetic field is projected in a certain angle [15], with the presence of Brownian motion and thermophoresis parameter [16-19], affected by heat absorption and viscous dissipation [20, 21], subjected to the chemical reaction [21], influenced by activation energy [22], has a slip effect at the boundary [23], and with the presence of thermal radiation [23, 24]. In addition, the different boundary shape, such as the fluid flows towards a moving thin needle [25] and moving plate [26] has been described.

Looking at the above-mentioned reported studies, the main purpose of this paper is to extend the model developed by Parvin *et al.,* [3] in 3D MHD Newtonian fluid over a flat horizontal stretching plane, into the inclined stretching plane. The method of this research works follows the following steps: 1) Develop the initial mathematical formulation by adding the effect of the inclination angle in the previous model [3], 2) Convert the formulation in (1) in the form of ordinary differential equations (ODEs), 3) Solve the ODEs by implementing the Matlab bvp4c coding. The characteristics of the Newtonian fluid flow, heat and mass transfers are obtained in the form of graphical illustrations, such as the respective profiles (velocity, temperature, concentration) and physical parameters (skin friction coefficient, local Nusselt number, local Sherwood number). All the numerical results are obtained from bvp4c technique through Matlab program.

## 2. Methodology

The magnetohydrodynamics (MHD) Newtonian flow over a three-dimensional horizontal inclined stretching plane (*x*-, *y,* and *z*- axes) is considered. The in or out direction is the vector *x*, *y* for horizontal and *z* is for vertical. The magnetic field vector is located at *z*- axis. The Newtonian fluid is assumed to be incompressible and electrically conducting, and the fluid model is shown in Figure 1. The initial mathematical formulation from Parvin *et al.,* [3], together with the effect of inclination angle acts on the stretching plane [27] are as follows:

$$\frac{\partial u}{\partial x}+\frac{\partial v}{\partial y}+\frac{\partial w}{\partial z}=0, \tag{1}$$

$$u\frac{\partial u}{\partial x}+v\frac{\partial u}{\partial y}+w\frac{\partial u}{\partial z}=v\frac{\partial^2 u}{\partial z^2}+g\beta_T\left(T-T_\infty\right)\cos\theta+g\beta_C\left(C-C_\infty\right)\cos\theta-\frac{\sigma B_0^2}{\rho}u, \tag{2}$$

$$u\frac{\partial v}{\partial x}+v\frac{\partial v}{\partial y}+w\frac{\partial v}{\partial z}=\nu\frac{\partial^2 v}{\partial z^2}+g\beta_T\left(T-T_\infty\right)\cos\theta+g\beta_C\left(C-C_\infty\right)\cos\theta-\frac{\sigma B_0^2}{\rho}u, \tag{3}$$

$$u\frac{\partial T}{\partial x}+v\frac{\partial T}{\partial y}+w\frac{\partial T}{\partial z}=\alpha\frac{\partial^2 T}{\partial z^2}+\frac{DK}{C_sC_p}\frac{\partial^2 C}{\partial z^2}, \tag{4}$$

$$u\frac{\partial C}{\partial x}+v\frac{\partial C}{\partial y}+w\frac{\partial C}{\partial z}=D\frac{\partial^2 C}{\partial z^2}+\frac{DK}{T_m}\frac{\partial^2 T}{\partial z^2}, \tag{5}$$

The velocity in the *x*-axis, the velocity in the *y*-axis, the velocity in z-axis, kinematic viscosity, inclination angle which plane *xy* is projected from *z*-axis, acceleration due to gravity, electrical conductivity, thermal diffusivity, coefficient of thermal expansion, coefficient of concentration expansions, uniform strength of magnetic field, mass diffusivity, thermal diffusion ratio, temperature of the fluid, concentration of the fluid, concentration susceptibility, specific heat at constant pressure, and mean fluid temperature are defined as these symbols: $u, v, w, \nu, \rho$, $\theta$, $g, \sigma, \alpha, \beta_T, \beta_C, \beta_0, D, K, T, C, C_g, C_p, T_m$.

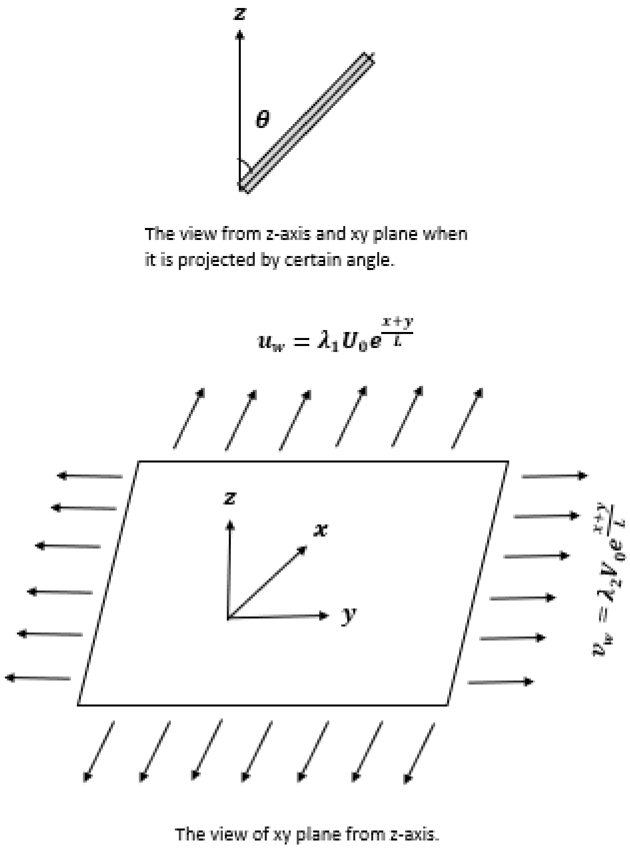


**Fig. 1.** Physical configuration with coordinate system

The related boundary conditions are [3]

At $z=0$ (at the surface is indicated by the subscript "$w$"):

The fluid velocity in $x$- axis: $u = u_w(x,y) = \lambda_1 U_0 e^{\frac{x+y}{L}}$,

The fluid velocity in $y$- axis: $v = v_w(x,y) = \lambda_2 V_0 e^{\frac{x+y}{L}} = \lambda_2 U_0 e^{\frac{x+y}{L}}$,

$(U_0 = V_0)$, $U_0 > 0$ and $V_0 > 0$.

The fluid velocity in z- axis: $w = W(x,y)$,

The temperature of the fluid: $T_w(x,y) = T_\infty + T_0 e^{\frac{x+y}{2L}}$,

The concentration of the fluid: $C_w(x,y) = C_\infty + C_0 e^{\frac{x+y}{2L}}$

As $z \to \infty$ (at adjacent point is indicated by the subscript "$\infty$"):

$$u \to 0, \quad v \to 0, \quad T \to T_\infty \quad C \to C_\infty \tag{6}$$

From Eq. (6), the reference length, stretching parameter in the $x$- axis, the stretching parameter in $y$-axis, and the wall mass suction velocity are expressed by the following symbols: $L,\ \lambda_1 > 0,\ \lambda_2 > 0,\ W(x,y)$.

The similarity transformations regarding to the mathematical formulation [3] as in Eq. (1) - Eq. (5) are

$$\eta = \sqrt{\frac{U_0}{2Lv}} e^{\frac{x+y}{2L}} z, \qquad u = U_0 e^{\frac{x+y}{L}} f_\eta, \qquad v = V_0 e^{\frac{x+y}{L}} h_\eta,$$

$$w = -\sqrt{\frac{vU_0}{2Lv}} e^{\frac{x+y}{2L}} \left[ f + \eta f_\eta + h + \eta h_\eta \right], \tag{7}$$

$$T = T_w(x,y) = T_\infty + T_0 e^{\frac{x+y}{2L}} \theta, \qquad C = C_w(x,y) = C_\infty + C_0 e^{\frac{x+y}{2L}} \phi,$$

where subscript $\eta$ indicates the differentiation with respect to $\eta$.

The following equations are produced from the substitution of Eq. (7) to Eq. (2) - Eq. (6):

$$f_{\eta\eta\eta} - 2\left[f_\eta\right]^2 - 2h_\eta f_\eta + f_{\eta\eta} f_\eta + f_{\eta\eta} h_\eta + 2\left(Ri_x\right) \times \left\{\vartheta + N\varphi\right\} cos\vartheta - 2Hf_\eta = 0 \tag{8}$$

$$h_{\eta\eta\eta} - 2\left[h_\eta\right]^2 - 2f_\eta h_\eta + h_{\eta\eta} h_\eta + h_{\eta\eta} f_\eta + 2\left(Ri_y\right) \times \left\{\theta + N\phi\right\} \cos\theta - 2Hh_\eta = 0 \tag{9}$$

$$\frac{1}{Pr}\theta_{\eta\eta} - \theta\left(f_\eta + h_\eta\right) + \theta_\eta\left(f + h\right) + \left(Db\right) f_{\eta\eta} = 0 \tag{10}$$

$$\frac{1}{Sc}\phi_{\eta\eta} - \phi\left(f_\eta + h_\eta\right) + \phi_\eta\left(f + h\right) + \left(Sr\right) f_{\eta\eta} = 0 \tag{11}$$

$$
\begin{aligned}
&\text{At } \eta = 0: \\
&f = S, \quad h = 0, \quad \theta = 1, \\
&f_\eta = 1, \quad h_\eta = \lambda_2 = \lambda, \quad \phi = 1. \\
&\text{As } \eta \to \infty: \\
&f_\eta \to 0, \quad h_\eta \to 0, \quad \theta \to 1, \quad \phi \to 1.
\end{aligned} \tag{12}
$$

Where the stretching rate at *y*-axis $\lambda_2$ is equal to $\lambda$.

The parameters occurred in Eq. (8) - Eq. (12) are tabulated in Table 1. In this model, $U_0 = V_0$, then $Ri_x = Ri_y$. As a result, the mixed convection parameter for the *x*- and *y*- axes is denoted by *Ri*. The opposing flow is classified by negative *Ri*, whereas the assisting flow is positive *Ri.*

**Table 1**
The related governing parameters in ODEs

| Governing Parameters | Equations |
|---|---|
| Thermal Grashof number | $Gr_x = g\left(\beta_T\right)_f T_0 L^3 e^{\frac{x+y}{2L}} / \nu_f^2$ |
| Reynolds number in *x*-axis | $Re_x = U_0 L e^{\frac{x+y}{L}} / \nu_f$ |
| Reynolds number in *y*-axis | $Re_y = V_0 L e^{\frac{x+y}{L}} / \nu_f$ |
| Mixed convection in *x*-axis | $Ri_x = Gr_x / Re_x^2$ |
| Mixed convection in *y*-axis | $Ri_y = Gr_x / Re_y^2$ |
| Buoyancy ratio | $N = \left(\beta_C\right)_f \left(C_0\right) / \left(\beta_T\right)_f \left(T_0\right)$ |
| Magnetic field | $H = \left(\sigma L B_0^2\right) / \left(U_0 \rho e^{\frac{x+y}{L}}\right)$ |
| Prandtl number | $Pr = \nu / \alpha$ |
| Schmidt number | $Sc = \nu / D$ |
| Soret number | $Sr = DKT_0 / T_m C_0 \nu$ |
| Dufour number | $Db = \left(DKC_0\right) / \left(C_s C_p T_0 \nu\right)$ |
| Suction parameter | $S = -\sqrt{2L/U_0 \nu} e^{-\frac{x+y}{2L}} W\left(x, y\right)$ |

The physical parameters of skin friction coefficient $C_f$, local Nusselt number $Nu_x$ and local Sherwood number $Sh_x$ [3] are

$$
C_{fx}(\text{in } x\text{-axis}) = \frac{\tau_x}{\rho U_0^2}, \qquad C_{fy}(\text{in } y\text{-axis}) = \frac{\tau_y}{\rho U_0^2},
$$

$$
Nu_x = \frac{-L}{\left(T_w - T_\infty\right)} \left(\frac{\partial T}{\partial z}\right)_{z=0}, \; Sh_x = \frac{L}{\left(C_w - C_\infty\right)} \left(-\frac{\partial C}{\partial z}\right)_{z=0} \tag{13}
$$

Where $\tau$ is the wall shear stress. The subscript $x$ and $y$ in $\tau$ are according to the $x$- and $y$-axes. By implementing similarity transformation Eq. (7) into Eq. (13), then we obtain

$$\sqrt{2Re_x}\, e^{\frac{-2(x+y)}{L}} C_{fx} + \frac{1}{2Re_x} = f_{\eta\eta}(0), \qquad \sqrt{2Re_y}\, e^{-\frac{2(x+y)}{L}} C_{fy} + \frac{1}{2Re_y} = h_{\eta\eta}(0),$$

$$Nu_x \sqrt{\frac{2}{Re_x}} = -\theta_\eta(0), \quad Sh_x \sqrt{\frac{2}{Re_x}} = -\phi_\eta(0) \tag{14}$$

From the reduction of Eq. (13) to Eq. (14), the skin friction coefficient in $x$-axis, the skin friction coefficient in $y$-axis, local Nusselt number, and local Sherwood now will be expressed as $f_{\eta\eta}$ (0), $h_{\eta\eta}$ (0), -θ(0), and -ϕ(0), respectively.

As a conclusion, the methodology in this section is presented as a flow chart in the Figure 2, starts from the mathematical formulation until the step to obtain the numerical solutions.

## 3. Results

As boundary layer is concerned, the impact of the mixed convection parameter *Ri*, magnetic parameter *H*, Dufour number *Db* and Soret number *Sr* on the boundary are believed to give pertinent impact. The existence of these parameters in Eq. (8) – Eq. (12) are the main focus of this study. As such, we opt to solve those equations by using Matlab bvp4c method. For the sake of understanding the influence of these parameters on the horizontal velocity $f_\eta$, vertical velocity $h_\eta$, temperature profile θ and concentration profile ϕ pictorial descriptions are presented in Figures 2 – 5 for this purpose, taking into account various arbitrary constants. Whilst, from an engineering point of interest, the skin friction coefficients in $x$- and $y$- axes ( $f_{\eta\eta}$ (0) and $h_{\eta\eta}$ (0)), local Nusselt number $-\theta_\eta(0)$ and local Sherwood number $-\phi_\eta(0)$ are portrayed in Figures 6 - 8 respectively. The values of the governing parameters used are as follows unless otherwise mentioned: $\theta = 30^\circ,\ Ri = 0.8,\ N = 3.0,\ H = 0.5,\ Pr = 1,\ Db = 0.5,\ Sc = 0.5,\ Sr = 0.2,\ S = 1.0,\ \lambda = 0.5.$

The comparison on the $\theta_\eta(0)$ data for the various Prandtl number Pr when the model is reduced to a flat horizontal stretching plane $(\theta = 0^\circ)$ is tabulated in Table 2. The previous investigator reported the rate of heat transfer when *Pr* = 1,3,5. However, the additional numerical values for the comparison are for *Pr* = 2,4. The data in this table shows good agreement with the previous report [3]. Therefore, it is clear that all the profiles satisfy the related boundary conditions, and this comparison gives us the confident to proceed with the subsequent numerical calculations.

The imposition of *H* in the fluid flow is seen to decrease the velocity along the horizontal and vertical components, i.e. $f_\eta$ and $h_\eta$ as depicted in Figures 3(a) and 3(b), respectively. As a result of magnetic field appearance, the Lorentz force will retard the flow motion. This in turn, results in the velocity reduction. Both profiles show that the velocity starts at a certain value and slowly decreases to 0 once the boundary layer is fully formed as agreed in boundary conditions Eq. (12).

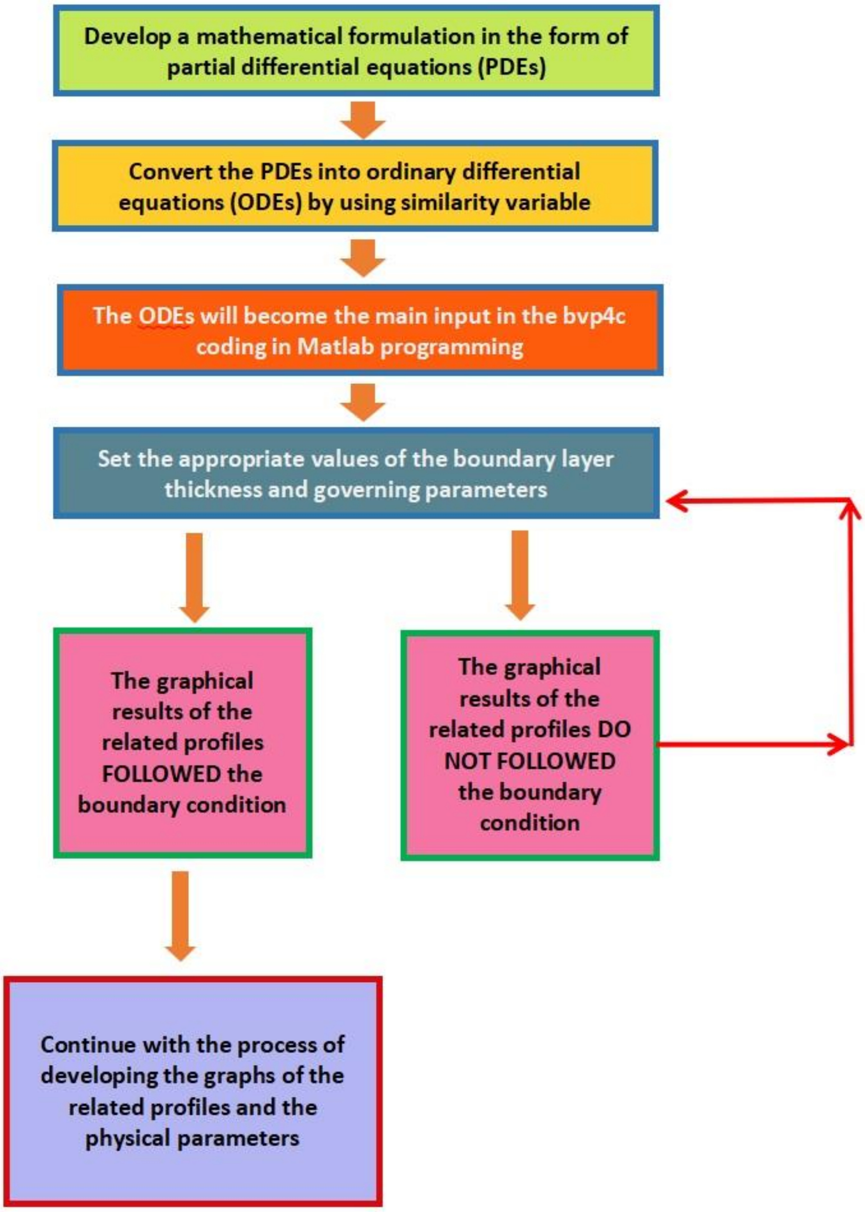


**Fig. 2.** Flow chart of the methodology process for the Newtonian fluid flow model in this paper

Figures 4(a) and 4(b) illustrates the repercussion of the stretching parameter $\lambda$ towards the horizontal and vertical velocity profiles ($f_\eta$ and $h_\eta$). It is found that $\lambda$ has no significant changes on the $f_\eta$ as the decrement is too small. However, the increment of $\lambda$ is notable in the $h_\eta$ only near the surface ($\eta \ll 1$) due to the fixed $\lambda$ as specified in the boundary condition Eq. (12). Here, the vertical velocity increases as $\lambda$ increases and beyond $\eta > 1$, $\lambda$ is seen to be less powerful, but somehow decreases the vertical velocity component even with diminutive changes.

The impact of *Db* on the $\theta$ and $\phi$ profiles are portrayed in Figures 5(a) and (b) respectively. Remarkable impact is seen to ensue on the temperature profile. The accretion of *Db* results in the increment of temperature and thickness of the boundary layer as can be seen in Figure 5(a). However, the increment of *Db* gives a trifling influence on the concentration profile. As mathematical point of interest is concerned, it is worth to mention that for $\eta \ll 2.5$ approximately, the concentration is slightly lower as Db increases and the trend contradicts as $\eta > 2.5$.

**Table 2**
The comparison on wall-temperature gradient $\theta_\eta(0)$ for a flat horizontal stretching plane

| $\lambda$ | Pr | Parvin *et al.,* [3] | Present |
|---|---|---|---|
| | 1 | -1.00139 | -1.00140 |
| | 2 | - | 1.54325 |
| 1.1 | 3 | -1.96030 | -1.96028 |
| | 4 | - | 2.31209 |
| | 5 | -2.62216 | -2.62214 |
| | 1 | -0.95478 | -0.95481 |
| | 2 | - | -1.47142 |
| 1 | 3 | -1.86907 | -1.86904 |
| | 4 | - | -2.20449 |
| | 5 | -2.50013 | -2.50011 |
| | 1 | 0.90579 | -0.90583 |
| | 2 | - | -1.39590 |
| 0.9 | 3 | 1.77316 | -1.77312 |
| | 4 | - | -2.09135 |
| | 5 | -2.37183 | -2.37180 |

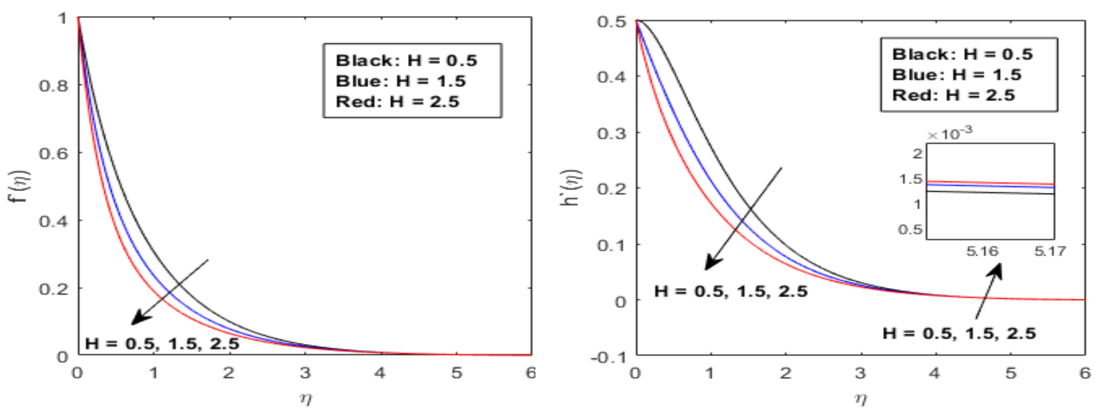


(a) (b)

**Fig. 3.** The (a) $f_\eta$ and (b) $h_\eta$ profiles for various values of $H$

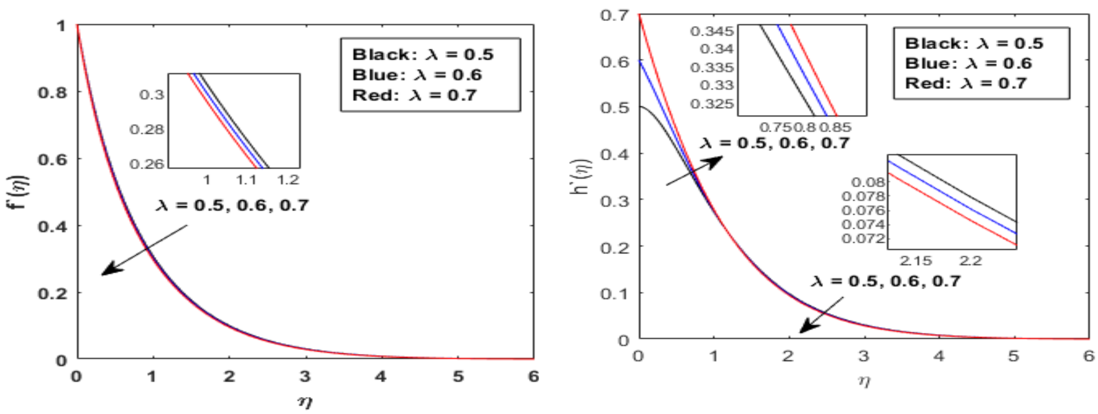


(a) (b)

**Fig. 4.** The (a) $f_\eta$ and (b) $h_\eta$ profiles for various values of $\lambda$

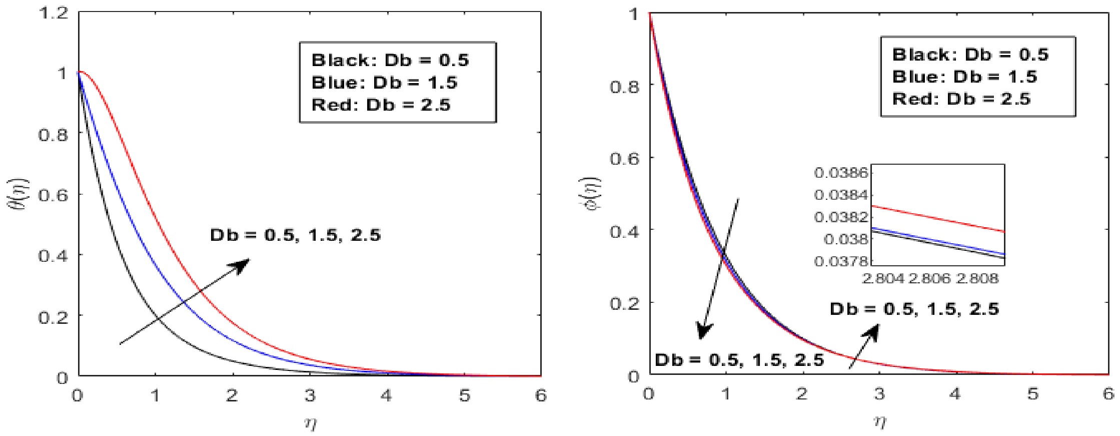


(a) (b)

**Fig. 5.** The (a) $f_\eta$ and (b) $h_\eta$ profiles for various values of *Db*

Figures 6(a) and (b) presented the influence of Soret number *Sr* in the fluid flow on the θ and ϕ profiles, respectively. The impact of the *Sr* number on the temperature is more dominant for $\eta \ll 1.5$ as depicted in Figure 6(a). Here, the increment of *Sr* number results in lowering the temperature and is no longer valid beyond this value $\eta > 1.5$. Nevertheless, it is observed that the impact of *Sr* number is to enhance the temperature even with slight changes at $\eta > 1.5$. As per concentration, the rise in *Sr* number enhances the concentration and in fact, higher *Sr* number (*Sr* = 2.2) inspires an overshoot profile near the sheet, showing that the concentration comes to its maximum value before asymptotically goes to 0 to achieve a certain thickness.

Above all, *Db* and *Sr* numbers have opposite behaviour. i.e the *Db* effect is discovered to wield huge influence on the θ profile as compared to the ϕ profile, and contrary behavior occurred for the *Sr* number. Increasing Dufour number causes the increment in the concentration gradient. Therefore, mass diffusion rate becomes faster and the thermal energy is distributed to all the particles. As a result, the temperature profile enhances. On the other hand, the Soret number causes the concentration profile to increase due to the enlargement of temperature gradient. This gradient is associated with the mass energy and consequently, the concentration profile is augmented.

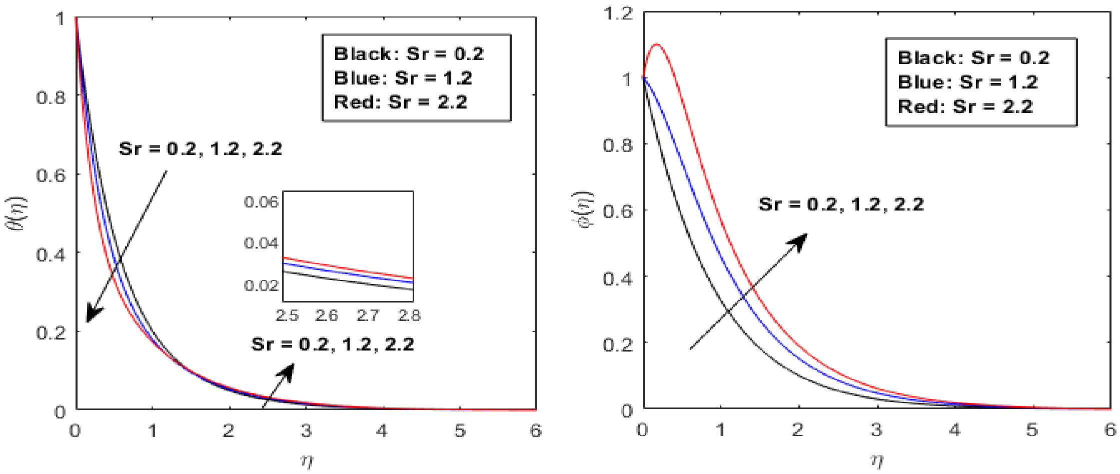


(a) (b)

**Fig. 6.** The (a) θ and (b) ϕ profiles for various values of *Sr*

The skin friction coefficients in *x*- and *y*- axes ($f_{\eta\eta}(0)$ and $h_{\eta\eta}(0)$), local Nusselt number $-\theta_\eta(0)$ and local Sherwood number $-\phi_\eta(0)$ have been plotted in Figures 7-9, and been tabulated in Table 3 for various $\lambda$, *H, Db* and *Sr.* The impact of $\lambda$ is seen to decrease both magnitude of horizontal and vertical skin frictions and the same trend takes place as the magnetic effect increases on the fluid flow as can be viewed in Figure 7. Comparatively, at fixed $\lambda$, the magnitude of the skin friction along the vertical sheet (Figure 7b) is seen to have massive value in contrast with the horizontal skin friction (Figure 7a). In spite of that, the skin frictions are noted to have negative values due to the buoyancy force which opposes the fluid flow.

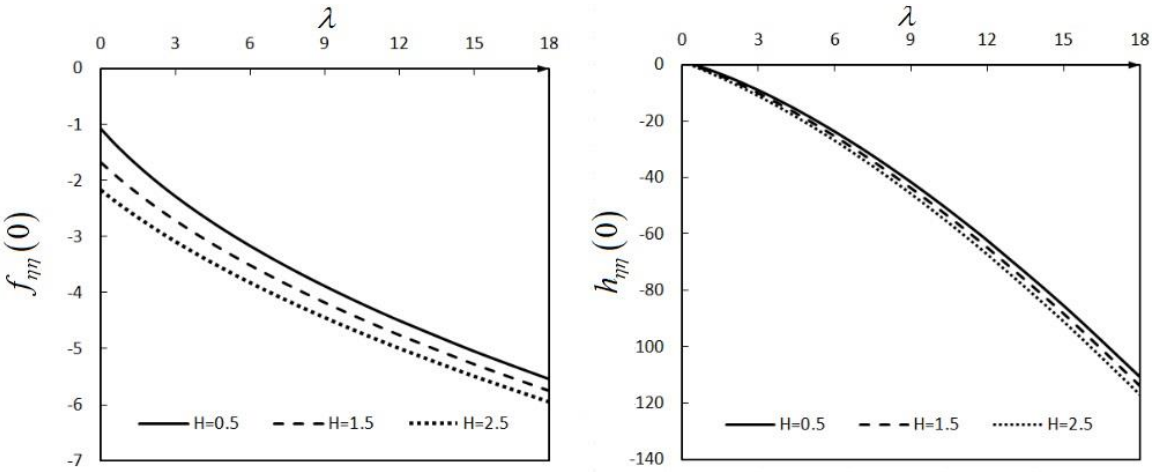


(a) (b)

**Fig. 7.** The (a) horizontal $f_{\eta\eta}(0)$ and (b) vertical $h_{\eta\eta}(0)$ sheets for various values of $\lambda$ and *H*

**Table 3**
The values of skin friction coefficients $f_{\eta\eta}(0)$, local Nusselt number $-\theta_\eta(0)$ and local Sherwood number $-\phi_\eta(0)$ for various *λ, H, Sr, Db*

| $\lambda$ | H | Db | Sr | $f_{\eta\eta}(0)$ | $h_{\eta\eta}(0)$ | $-\theta_\eta(0)$ | $-\phi_\eta(0)$ |
|---|---|---|---|---|---|---|---|
| | 0.5 | 0.5 | 0.2 | -1.31246 | -0.00099 | 1.64539 | 1.06645 |
| | | | 0.6 | -1.25924 | 0.05890 | 1.78404 | 0.79020 |
| 0.5 | | | 1.0 | -1.20459 | 0.12001 | 1.95012 | 0.45144 |
| | | 0.7 | | -1.20292 | 0.12201 | 1.92025 | 0.46256 |
| | | 0.9 | | -1.20129 | 0.12398 | 1.88783 | 0.47463 |
| | 0.7 | | | -1.32581 | 0.03914 | 1.87300 | 0.46179 |
| | 0.9 | | | -1.44526 | -0.04143 | 1.85887 | 0.44961 |
| 0.7 | | | | -1.52681 | -0.66520 | 1.90513 | 0.45983 |
| 0.9 | | | | -1.60623 | -1.31273 | 1.95023 | 0.46998 |

The influence of *Sr* and *Db* numbers on the local Sherwood and Nusselt numbers are drawn in Figure 8 and Figure 9 respectively. As Sr number increases, the Sherwood number given by $-\phi_\eta(0)$ is found to decrease except for *Db* = 2.5, where contrary behavior is observed. High Sherwood number indicates that mass transfer is dominant while a low Sherwood number indicates that molecular diffusion is dominant. At low *Sr* number, the phenomenon of *Db* is seen to decrease the local Nusselt number. However, *Db* seems to be ineffectual when *Sr* = 1.2. As *Sr* increases and with the increment of the *Db* number, the local Nusselt number is found to enhance as well, and the increment is very much remarkable for $Db >> 0.8$. Soret number is the ratio of temperature difference to the concentration. Hence, the bigger $Sr$ number stands for a larger temperature difference and precipitous gradient [28].

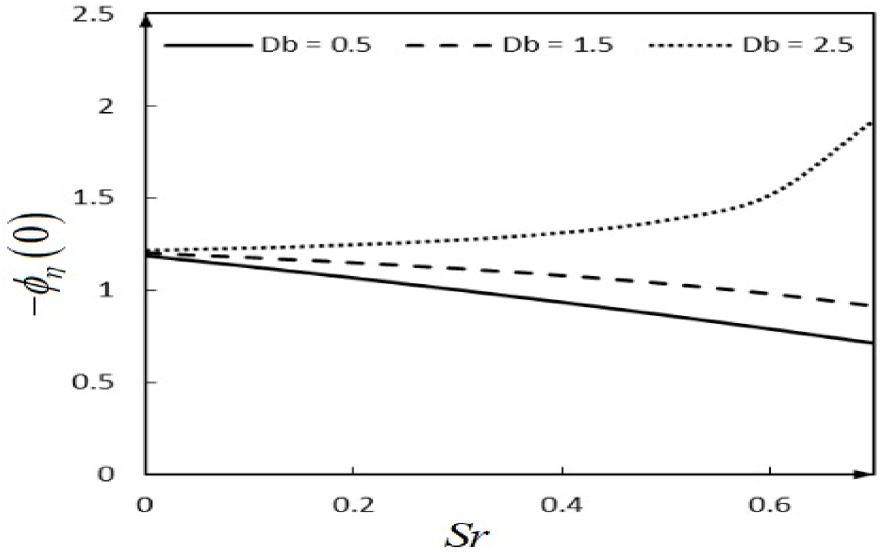


**Fig. 8.** The variation of $-\phi_\eta(0)$ for several values of *Sr* and *Db* numbers

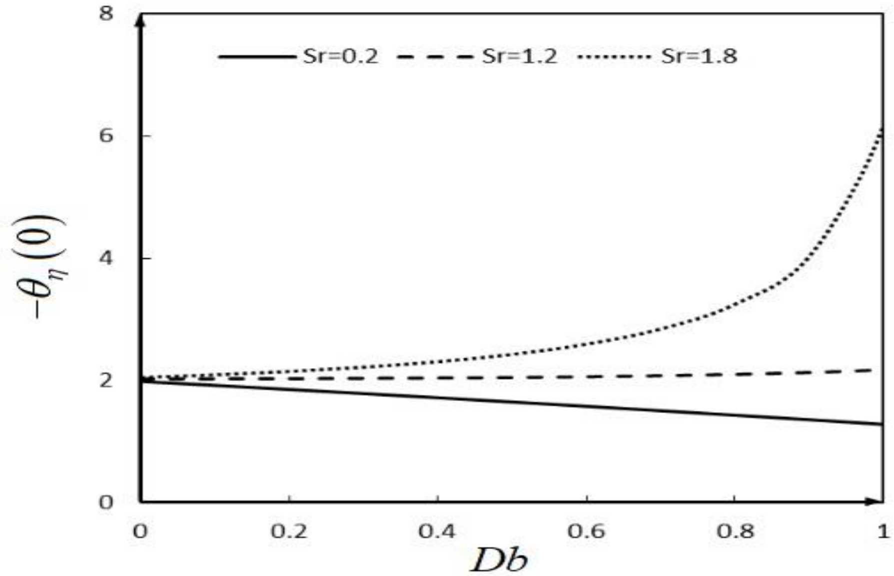


**Fig. 9.** The variation of $-\theta_\eta(0)$ for several values of *Sr* and *Db* numbers

## 4. Conclusions

The influence of the mixed convection parameter, magnetic parameter, Dufour number and Soret number on the three-dimensional Newtonian fluid over an inclined plate is thoroughly investigated. The effect of inclination angle is added to the previous Newtonian fluid flow model [3]. The graphs are plotted for the the velocity, temperature, and concentration profiles. In addition, the skin frictions along the horizontal and vertical sheets, local Sherwood number and local Nusselt number are also illustrated. It can be inferred that the magnetic parameter is seen to decrease the velocity in both directions which in turn decreases the skin frictions. Whilst the increment of Dufour number is noticed to increase the temperature and the local Sherwood number. The rise of Soret number results in the rise of concentration which leads to the addition of local Nusselt number.

**Acknowledgement**
This research is fully supported by PILOT grant, (UNI/C09/PILOT/85088/2022) from Universiti Malaysia Sarawak. Support from the Centre of Pre-University Universiti Malaysia Sarawak are also acknowledged.

**References**
[1] Ahmad, Shafiq, Hasan Huseyin Coban, Muhammad Naveed Khan, Umair Khan, Qiu-Hong Shi, Taseer Muhammad, Ronnason Chinram, and Seifedine Kadry. "Computational analysis of the unsteady 3D chemically reacting MHD flow with the properties of temperature dependent transpose suspended Maxwell nanofluid." *Case Studies in Thermal Engineering* 26 (2021): 101169. https://doi.org/10.1016/j.csite.2021.101169
[2] Odesola, A. S., I. O. Abiala, M. G. Sobamowo, and O. J. Fenuga. "Transient three-dimensional magnetohydrodynamic flow of heat and mass transfer of a Casson nanofluid past a stretching sheet with non-uniform heat source/sink, thermal radiation and chemical reaction." *Journal of Engineering and Thermal Sciences* 2, no. 2 (2022): 100-113. https://doi.org/10.21595/jets.2022.22815
[3] Parvin, S., S. S. P. M. Isa, and S. K. Soid. "THREE-DIMENSIONAL MODEL OF DOUBLE DIFFUSIVE MAGNETOHYDRODYNAMIC NEWTONIAN FLUID FLOW." *Magnetohydrodynamics (0024-998X)* 57, no. 3 (2021). https://doi.org/10.22364/mhd.57.3.6
[4] Nagalakshmi, P. S. S., N. Vijaya, and Shaik Mohammed Ibrahim. "Entropy Generation of Three-Dimensional Williamson Nanofluid Flow Explored with Hybrid Carbon Nanotubes over a Stretching Sheet." *CFD Letters* 15, no. 7 (2023): 112-130. https://doi.org/10.37934/cfdl.15.7.112130
[5] Teh, Yuan Ying, and Adnan Ashgar. "Three dimensional MHD hybrid nanofluid Flow with rotating stretching/shrinking sheet and Joule heating." *CFD Letters* 13, no. 8 (2021): 1-19. https://doi.org/10.37934/cfdl.13.8.119
[6] Teh, Yuan Ying, and Adnan Ashgar. "Three dimensional MHD hybrid nanofluid Flow with rotating stretching/shrinking sheet and Joule heating." *CFD Letters* 13, no. 8 (2021): 1-19. https://doi.org/10.37934/cfdl.13.8.119
[7] Hussain, Azad, Mubashar Arshad, Aysha Rehman, Ali Hassan, S. K. Elagan, Hijaz Ahmad, and Amira Ishan. "Three-dimensional water-based magneto-hydrodynamic rotating nanofluid flow over a linear extending sheet and heat transport analysis: A numerical approach." *Energies* 14, no. 16 (2021): 5133. https://doi.org/10.3390/en14165133
[8] Ilias, Mohd Rijal, Nur Sa'aidah Ismail, Nurul Hidayah AbRaji, Noraihan Afiqah Rawi, and Sharidan Shafie. "Unsteady aligned MHD boundary layer flow and heat transfer of a magnetic nanofluids past an inclined plate." *International Journal of Mechanical Engineering and Robotics Research* 9, no. 2 (2020): 197-206.
[9] Raza, Ali, Umair Khan, Zehba Raizah, Sayed M. Eldin, Abeer M. Alotaibi, Samia Elattar, and Ahmed M. Abed. "Numerical and computational analysis of magnetohydrodynamics over an inclined plate induced by nanofluid with Newtonian heating via fractional approach." *Symmetry* 14, no. 11 (2022): 2412. https://doi.org/10.3390/sym14112412
[10] Osman, Husna Izzati, Nur Fatihah Mod Omar, Dumitru Vieru, and Zulkhibri Ismail. "A Study of MHD Free Convection Flow Past an Infinite Inclined Plate." *Journal of Advanced Research in Fluid Mechanics and Thermal Sciences* 92, no. 1 (2022): 18-27. https://doi.org/10.37934/arfmts.92.1.1827
[11] Kaushik, Preeti, and Upendra Mishra. "Numerical solution of free stream MHD flow with the effect of velocity slip condition from an inclined porous plate." *J. Math. Comput. Sci.* 12 (2021): Article-ID. https://doi.org/10.28919/jmcs/6913
[12] Sulochana, Chalavadi, Sultana Begum, and Tirumala Prasanna Kumar. "MHD Mixed Convective Non-Newtonian Stagnation Point Flow Over an Inclined Stretching Sheet: Numerical Simulation." *Journal of Advanced Research in Fluid Mechanics and Thermal Sciences* 102, no. 1 (2023): 73-84. https://doi.org/10.37934/arfmts.102.1.7384
[13] Begum, Tahera, Geetan Manchanda, Arshad Khan, and Naseem Ahmad. "On numerical solution of boundary layer flow of viscous incompressible fluid past an inclined stretching sheet in porous medium and heat transfer using spline technique." *MethodsX* 10 (2023): 102035. https://doi.org/10.1016/j.mex.2023.102035

[14] Rehman, M. Israr Ur, Haibo Chen, Aamir Hamid, Sajid Qayyum, Wasim Jamshed, Zehba Raizah, Mohamed R. Eid, and El Sayed M. Tag El Din. "Soret and Dufour influences on forced convection of Cross radiative nanofluid flowing via a thin movable needle." *Scientific Reports* 12, no. 1 (2022): 18666. https://doi.org/10.1038/s41598-022-23563-5

[15] Parvin, Shahanaz, Siti Suzilliana Putri Mohamed Isa, Norihan Md Arifin, and Fadzilah Md Ali. "The inclined factors of magnetic field and shrinking sheet in Casson fluid flow, heat and mass transfer." *Symmetry* 13, no. 3 (2021): 373. https://doi.org/10.3390/sym13030373

[16] Rafique, Khuram, Muhammad Imran Anwar, Masnita Misiran, Ilyas Khan, Asiful H. Seikh, El-Sayed M. Sherif, and Kottakkaran Sooppy Nisar. "Brownian motion and thermophoretic diffusion effects on micropolar type nanofluid flow with Soret and Dufour impacts over an inclined sheet: Keller-box simulations." *Energies* 12, no. 21 (2019): 4191. https://doi.org/10.3390/en12214191

[17] Idowu, A. S., and B. O. Falodun. "Effects of thermophoresis, Soret-Dufour on heat and mass transfer flow of magnetohydrodynamics non-Newtonian nanofluid over an inclined plate." *Arab Journal of Basic and Applied Sciences* 27, no. 1 (2020): 149-165. https://doi.org/10.1080/25765299.2020.1746017

[18] Parvin, Shahanaz, Siti Suzilliana Putri Mohamed Isa, Wasim Jamshed, Rabha W. Ibrahim, and Kottakkaran Sooppy Nisar. "Numerical treatment of 2D-Magneto double-diffusive convection flow of a Maxwell nanofluid: Heat transport case study." *Case Studies in Thermal Engineering* 28 (2021): 101383. https://doi.org/10.1016/j.csite.2021.101383

[19] Parvin, Shahanaz, Siti Suzilliana Putri Mohamed Isa, Fuad S. Al-Duais, Syed M. Hussain, Wasim Jamshed, Rabia Safdar, and Mohamed R. Eid. "The flow, thermal and mass properties of Soret-Dufour model of magnetized Maxwell nanofluid flow over a shrinkage inclined surface." *PLoS One* 17, no. 4 (2022): e0267148. https://doi.org/10.1371/journal. pone.0267148

[20] Venkateswarlu, M., P. Bhaskar, and D. Venkata Lakshmi. "Soret and Dufour effects on radiative hydromagnetic flow of a chemically reacting fluid over an exponentially accelerated inclined porous plate in presence of heat absorption and viscous dissipation." *Journal of the Korean Society for Industrial and Applied Mathematics* 23, no. 3 (2019): 157-178. http://doi.org/10.12941/jksiam.2019.23.157

[21] Shukla, A. K., and Shubham Kumar Dube. "Numerical simulation of changes in Soret-Dufour number, Radiation, chemical reaction and viscous dissipation on unsteady MHD flow past an inclined porous plate embedded in porous medium with heat generation or absorption." (2022).

[22] Huang, J. S. "Chemical reaction and activation energy on heat and mass transfer for convective flow along an inclined surface in Darcy porous medium with Soret and Dufour effects." *Journal of Mechanics* 39 (2023): 88-104. https://doi.org/10.1093/jom/ufad006

[23] Najib, Najwa, Norfifah Bachok, Norihan Md Arifin, and Fadzilah Md Ali. "Stability analysis of stagnation-point flow in a nanofluid over a stretching/shrinking sheet with second-order slip, soret and dufour effects: A revised model." *Applied Sciences* 8, no. 4 (2018): 642. https://doi.org/10.3390/app8040642

[24] Sekhar, P. Raja, S. Sreedhar, S. Mohammed Ibrahim, and P. Vijaya Kumar. "Radiative Heat Source Fluid Flow of MHD Casson Nanofluid over A Non-Linear Inclined Surface with Soret and Dufour Effects." *CFD Letters* 15, no. 7 (2023): 42-60. https://doi.org/10.37934/cfdl.15.7.4260

[25] Salleh, Siti Nur Alwani, Norfifah Bachok, Norihan Md Arifin, and Fadzilah Md Ali. "Influence of Soret and Dufour on forced convection flow towards a moving thin needle considering Buongiorno's nanofluid model." *Alexandria engineering journal* 59, no. 5 (2020): 3897-3906. https://doi.org/10.1016/j.aej.2020.06.045

[26] Najib, Najwa, and Norfifah Bachok. "Boundary layer flow, heat and mass transfer of cu-water nanofluid over a moving plate with soret and dufour effects: Stability analysis." *Journal of Advanced Research in Fluid Mechanics and Thermal Sciences* 82, no. 1 (2021): 96-104. https://doi.org/10.37934/arfmts.82.1.96104

[27] Sarfraz, Mahnoor, and Masood Khan. "Thermodynamic irreversibility analysis of water conveying argentum and titania nanoparticles subject to inclined stretching surface." *Physica Scripta* 98, no. 2 (2023): 025205. https://doi.org/10.1088/1402-4896/acab92

[28] Srinivasacharya, D., B. Mallikarjuna, and R. Bhuvanavijaya. "Soret and Dufour effects on mixed convection along a vertical wavy surface in a porous medium with variable properties." *Ain Shams Engineering Journal* 6, no. 2 (2015): 553-564. https://doi.org/10.1016/j.asej.2014.11.007